Kovove Mater. 51 2013 53–61
DOI: 10.4149/km_2013_1_53

Corrosion failure and microstructure analysis of AISI 316L stainless steels for ship pipeline before and after welding

S. Kožuh[1]*, M. Gojić[1], L. Vrsalović[2], B. Ivković[3]

[1] *University of Zagreb, Faculty of Metallurgy, Aleja narodnih heroja 3, 44103 Sisak, Croatia*
[2] *University of Split, Faculty of Chemistry and Technology, Teslina 10/V, 21000 Split, Croatia*
[3] *Brodosplit Shipyard Ltd., Put Supavla 21, 21000 Split, Croatia*

Received 8 November 2011, received in revised form 24 September 2012, accepted 24 September 2012

Abstract

In the present study the corrosion behavior of AISI 316L stainless steel samples, taken from different parts of the ship pipeline, were investigated in chloride solutions. Research was conducted using gravimetric tests in 6 wt.% ferric chloride solution as well as cyclic potentiodynamic polarization measurements in 0.5 mol dm^{-3} NaCl solution. Additionally, the mechanism of corrosion attack developed on the steel surface was analyzed by optical microscopy, scanning electron microscopy (SEM) and energy dispersive X-ray (EDX) analysis. Microstructure analysis was performed before and after corrosion testing. The results showed that the lowest corrosion damage occurred on the base metal sample while the sample of interface of the *weld metal/heat affected zone* (WM/HAZ) had severe pitting damages. Inclusions were observed at the interface of the WM/HAZ, and this can be the main reason for pitting initiation.

K e y w o r d s: austenitic stainless steel, welding, pipeline failures, corrosion, cyclic polarization, microstructure

1. Introduction

Corrosion resistant austenitic stainless steels have a wide application as construction materials in chemical, food and petrochemical industry, medicine, etc., and one of the most important application areas is the development of various welded structures exposed to marine environment such as shipbuilding and offshore engineering [1–4]. Thus, the austenitic stainless steels are often used as a material for pipelines on ships for transport of various chemicals called "chemical tankers" [5]. High corrosion resistance of stainless steels is achieved through natural process of passivation – formation of the passive oxide film formed on their surfaces with the high chromium content. It is known that the high amounts of chromium in austenitic stainless steels improve the corrosion resistance [6]. However, chromium also can make the austenite unstable due to formation of chromium carbides and intermetallic phases during exposure to high temperatures (heat treatment or welding). Enhancement in protecting properties of surface oxide film on stainless steels surfaces can be achieved by their passivation in different solutions [2, 7–9]. Austenitic stainless steels exposed to chloride media are susceptible to the pitting corrosion, intergranular corrosion and stress corrosion cracking as localized corrosive attacks [10–12]. Changes occurred during welding (e.g. transformation in microstructure and residual stress) may worsen the corrosion properties [13, 14]. Also, Juraga et al. [1] mentioned that in less corrosive solution, under certain conditions, local depassivation and localized corrosion attacks may occur. These adverse situations may cause serious accidents, especially on products with thin walls (e.g. pipes and tanks). The literature often cites that corrosion related failures of components produced by welding of austenitic stainless steels are still common in engineering structures [10].

Corrosion failure of pipelines, made from AISI 316L stainless steel exposed to NaCl solution, on one chemical tanker, was the reason for conducting a detailed analysis of corrosion behavior and microstructure of different pipeline samples in NaCl solutions.

*Corresponding author: e-mail address: kozuh@simet.hr

Table 1. Chemical composition of AISI 316L stainless steel samples, wt.%

C	Si	Mn	P	S	Cr	Mo	Ni	Ti	Nb	Fe
0.02	0.47	1.23	0.045	0.009	16.64	2.53	10.68	0.007	0.024	rest

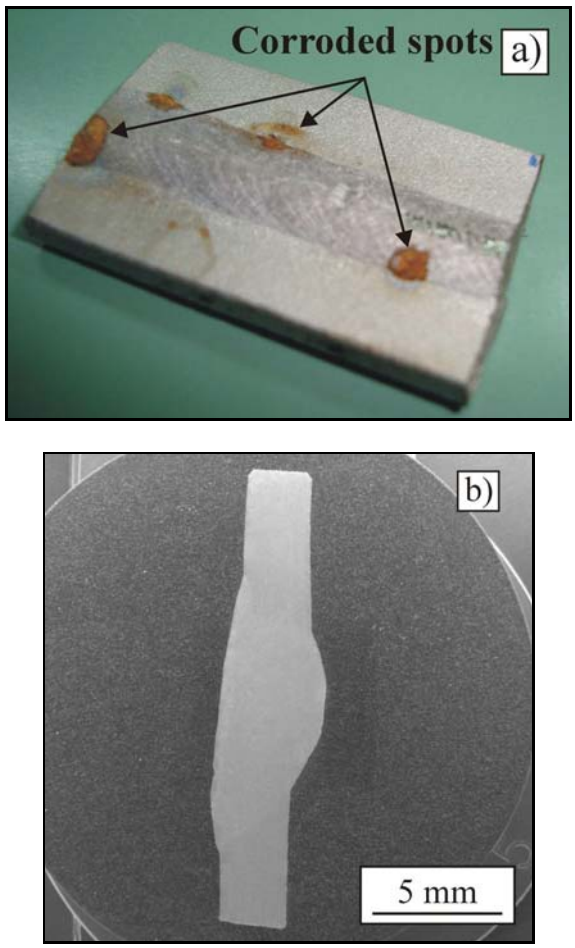

Fig. 1. Photograph of the as-received sample of the corroded welded joint (a) and the sample prepared for microstructural analysis before corrosion testing (b).

2. Experimental

The composition of the investigated AISI 316L stainless steel is given in Table 1. Figure 1a shows the actual photograph of as-received samples of the welded joint which was cut from the ship pipeline. Also, corroded spots can be observed in Fig. 1a. Figure 1b shows a sample of the welded joint before corrosion testing prepared for microstructural analysis. For better understanding of corrosion behavior of AISI 316L stainless steel in NaCl solution the morphologies of electrode surfaces after electrochemical testing were analyzed. Before and after the electrochemical testing the selected samples were investigated under light microscope (LM) and scanning electron microscope (SEM) equipped with energy dispersive spectrometer (EDX). Sample for microstructural analysis of the welded joint before corrosion testing was subsequently ground, polished and electrolytically etched. In order to expose austenite and ferrite boundaries, Kalling's No. 2 solution (5 g $CuCl_2$ + 100 ml HCl + 100 ml ethanol) was used. The delta ferrite content in the base and weld metals was determined by means of a ferritoscope. This method takes advantage of the fact that ferrite is magnetic and austenite is not.

Samples for corrosion testing were cut from the steel ship pipeline which was joined by TIG welding process with the austenite electrode (0.03 % C, 0.8 % Si, 18.5 % Cr, 2.6 % Mo, 12 % Ni, 66.07 % Fe, wt.%) in the argon inert atmosphere. The first sample was from the base metal (BM) of AISI 316L stainless steel which was not affected by the high temperature during the welding process. The second sample was the sample which included the interface of the *weld metal/heat affected zone* (WM/HAZ). Rectangular specimens (approximately $50 \times 20 \times 3\,mm^3$) were used for gravimetric measurements which were carried out in 6 wt.% $FeCl_3 \times 6\ H_2O$ solution thermostated on $20 \pm 1\,℃$ for a period of 72 h, according to the standard ASTM G-48 tests (practice A) [15]. Before the experiment, each sample was passivated for 60 min in the mixture of HNO_3 and HF which was prepared by mixing 475 ml of bidistilled water, 450 ml HNO_3 (65 %) and 75 ml of HF. The dry samples were weighed on the Metler Toledo model AB204-S analytical balance, with the precision of 0.1 mg. The samples were immersed into the $FeCl_3 \times 6\ H_2O$ solution for 72 h. Upon completion of the experiment, the samples were extracted, rinsed with bidistilled water, dried and finally weighed again at room temperature.

Electrochemical measurements (DC) were conducted with PAR 273A Potentiostat/Galvanostat. For electrochemical measurements the working electrodes were made by cutting the steel pipe square samples to dimensions of $12 \times 14\,mm^2$. An electrical contact was achieved by soldering insulated copper wire on the steel samples. All sides of the electrode except one were isolated with epoxy resin. The exposed geometric area was $1.62\,cm^2$. Before each experiment the electrode surface was mechanically polished with emery paper to a 1000 metallographic finish, degreased in ethanol, rinsed with double distilled water and immersed in the passivation solution for 60 min. After passivation, electrode was thoroughly rinsed with double distilled water and immersed in electrolyte ($0.5\,mol\,dm^{-3}$ NaCl solution). A three-electrode

cell was utilized, with the stainless steel working electrode, saturated calomel electrode (SCE) as the reference electrode and the platinum plate counter electrode. Potentiodynamic cyclic polarization measurements were performed at a scan rate of 1 $mV\,s^{-1}$, from –200 mV with respect of the corrosion potential (E_{corr}) and scanning back to the starting potential when the samples reached a current density value of 10^4 $\mu A\,cm^{-2}$. In order to perform tests in a deaerated solution, argon was bubbled through the solution 30 min prior to the electrode insertion into the solution, as well as during the experiments. All measurements were performed in quiescent solution at 20 ± 1 °C.

3. Results and discussion

The chemical composition of the investigated pipe from AISI 316L stainless steel is presented in Table 1. On the basis of it chromium and nickel equivalents can be determined. According to the Schaeffler diagram, chromium and nickel equivalents can be calculated by the equations [16]:

$$Cr_{eq} = \%\ Cr + 1.5\ \%\ Si + \%\ Mo + 0.5\ \%\ (Ta + Nb) + + 2\ \%\ Ti + \%\ W + \%\ V + \%\ Al, \quad (1)$$

$$Ni_{eq} = \%\ Ni + 30\ \%\ C + 0.5\ \%\ Mn + 0.5\ \%\ Co. \quad (2)$$

The microstructural analysis of the welded joint was performed before and after corrosion testing. As can be seen, the base metal microstructure differed from the microstructure of the weld metal (Fig. 2). Figure 2 shows an austenitic polygonal grain of AISI 316L stainless steel base metal with a low delta ferrite content. The final microstructure of the base metal, according to the Shaeffler diagram, consisted of austenite and about 1 % delta ferrite [16]. Stringers of delta ferrite can be seen elongated in the rolling direction. The delta ferrite content is important for predicting solidification mode of the weld metal [17]. The microstructure of the base metal was created by fully austenite solidification mode with 0.4 % delta ferrite which was measured by ferritoscope. The weld metal showed a dendritic microstructure. In accordance to the Shaeffler diagram and the weld metal Cr_{eq}/Ni_{eq} ratio (1.73), the delta ferrite content was about 10 %. Delta ferrite content measured with a ferritoscope was 10.6 %. The area of weld metal contained a continuous network of vermicular and lathy type of ferrite with ferrite-austenite solidification mode ($1.48 \leq Cr_{eq}/Ni_{eq} \leq 1.95$). As a consequence of the rapid cooling, a high content of delta ferrite in the dendritic boundary was observed. In the heat affected zone, when the base metal was heated but not melted, the typical austenitic microstructure was observed. The presence of 5–10 % delta ferrite in the weld metal is optimal to reduce hot cracking during solidification. At fully austenitic steel this cracking takes place due to segregation of impurity elements such as sulphur and phosphorus and leads to low melting point phases. However, this amount of delta ferrite, which is rich in chromium, could increase the uniform corrosion and pitting susceptibility. Figures 3–5 show the microstructure and EDX results of the constituents in the base

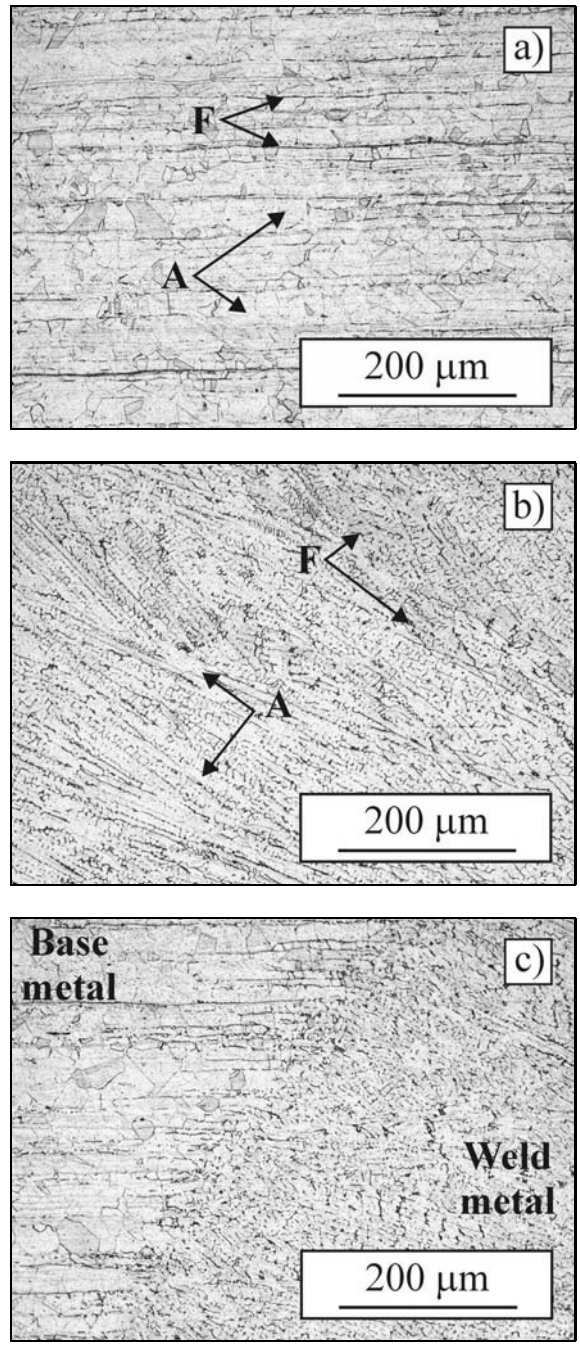

Fig. 2. Optical micrographs of AISI 316L stainless steel base metal (a), weld metal (b) and interface of the WM/HAZ (c) before corrosion testing; A – austenite, F – ferrite.

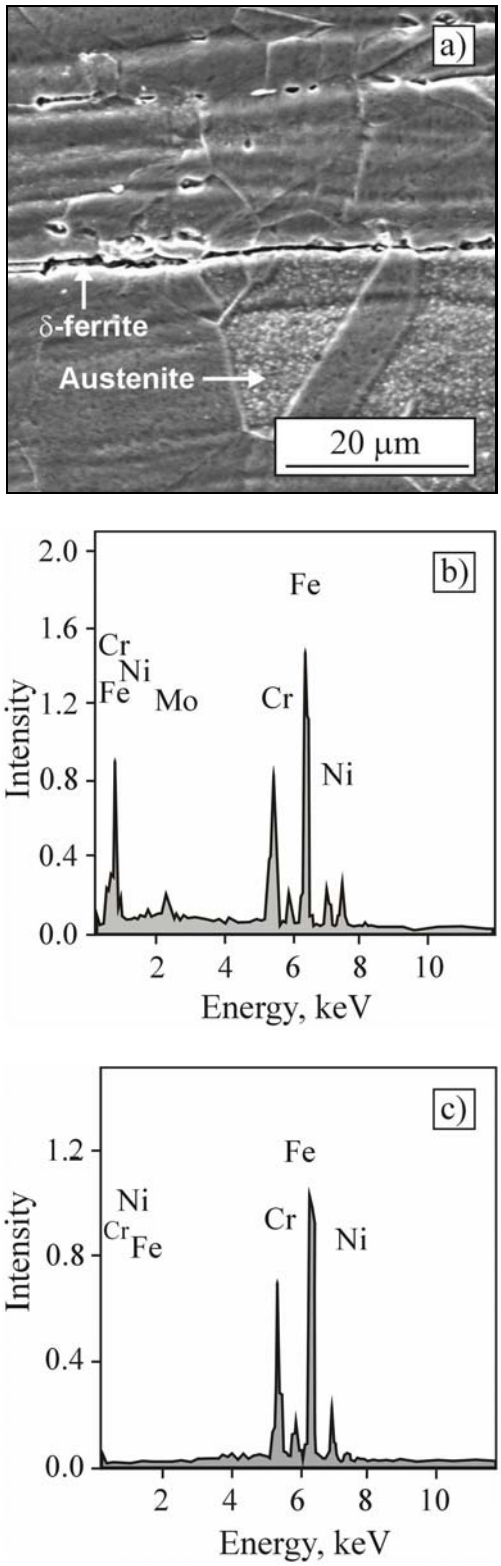

Fig. 3. SEM micrograph (a) of the base metal AISI 316L with the EDX spectrums of austenite (b) and delta ferrite (c).

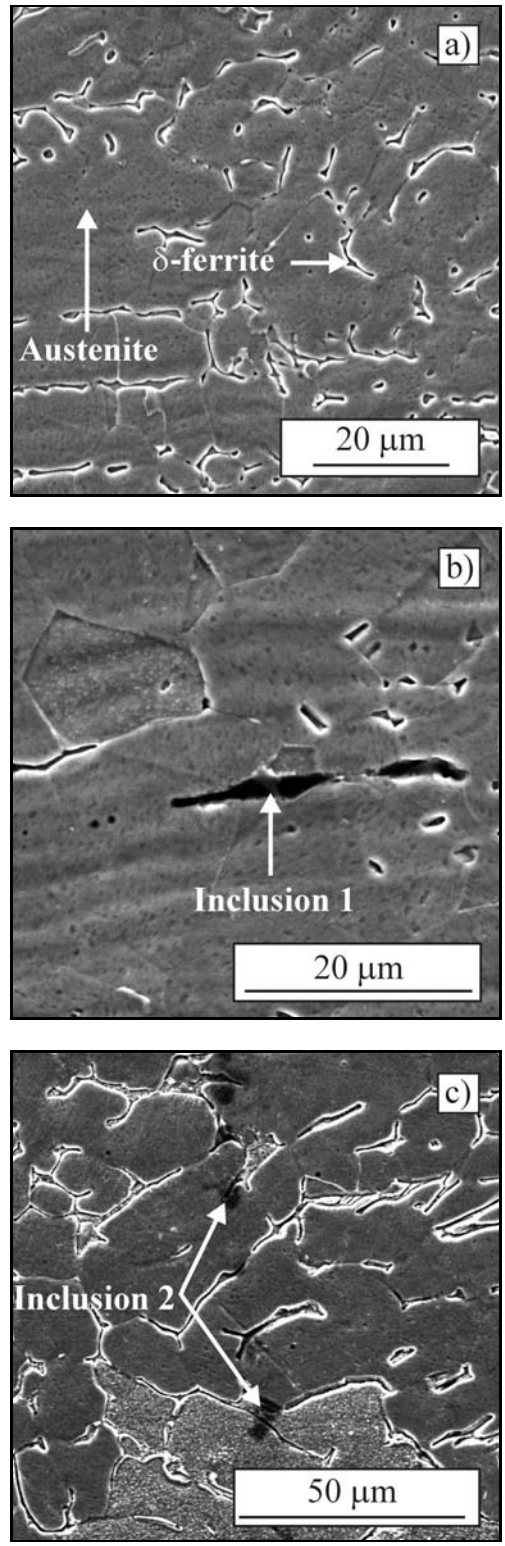

Fig. 4. SEM micrographs at the interface of the WM/HAZ of AISI 316L steel before corrosion testing.

metal and the WM/HAZ. Also, the EDX results of the different microstructure constituents are presented in Tables 2 and 3.

The variation of the mass loss obtained for the AISI 316L stainless steel samples which were exposed to 6 wt.% $FeCl_3 \times 6\ H_2O$ is shown in Table 4.

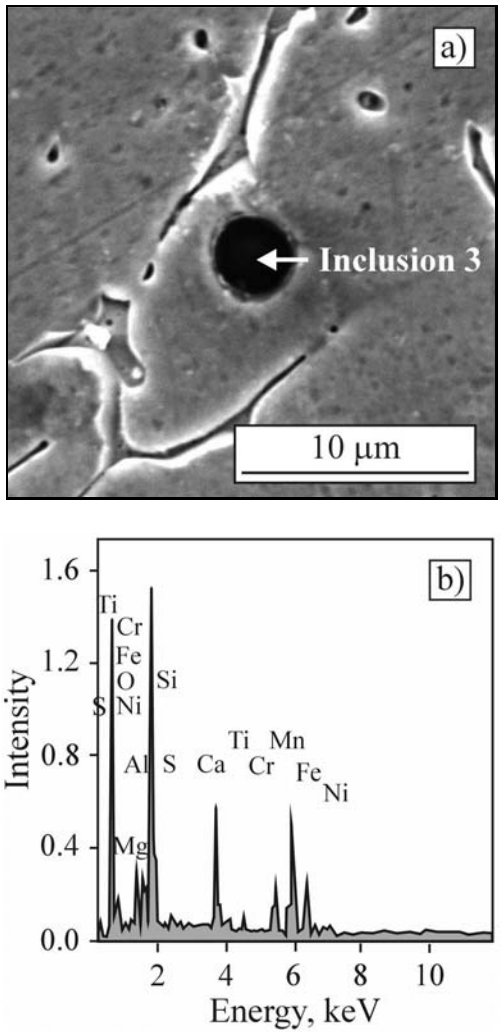

Fig. 5. SEM micrograph (a) and EDX spectrum (b) of inclusion in the weld metal AISI 316L before corrosion testing.

It can be seen from Table 4 that both samples experienced mass loss. The smallest weight loss was observed on the sample of the base metal, while the highest mass loss suffered at the interface of the WM/HAZ. This could be explained by the fact that the welding process induced some structural changes in the steel material which had negative effect to its corrosion resistance. After the gravimetric examination, a visual examination and photographic reproduction of specimens surfaces were taken, along with the optical microscopy examination specimen faces for pits at low-magnification (20×). Figure 6 shows the results of these examinations.

There are no visual pitting damages on the base metal sample, but pitting damages can be easily seen on samples of interface of the WM/HAZ. The corrosion attack on the sample of the WM/HAZ was concentrated in the places of heat tints which were located at the edge of the weld zone.

In some places at the surface of the samples some irregularities can be seen, such as indentations, small protrusions and places of heat tints, especially on the sample of the WM/HAZ. The above defects have occurred in the production and manipulation of pipes and are not caused by corrosion processes that occurred in chloride media, and can represent weak spots for the corrosion attack [1]. Such defects are usually present on marine pipelines after their installations. The results of these investigations can lead to the conclusion that the base metal has the highest resistance for pitting corrosion attack while the weld zone is susceptible to this form of local corrosion.

The results of the cyclic potentiodynamic polarization measurements, which were undertaken in 0.5 mol dm^{-3} NaCl solution, are presented in Fig. 7. The results of polarization studies are collected in Table 5, which comprises E_{corr}, primary passivation potential (E_{pp}), pitting potential (E_{pit}) and the repassivation potential (E_{rp}) values.

All cyclic potentiodynamic curves exhibited positive hysteresis. The pitting potential shifted towards more noble potentials for the base metal in respect to the WM/HAZ. The pitting potential was the highest

Table 2. Chemical composition of austenite and delta ferrite in the base metal of AISI 316L, wt.%

	Fe	Cr	Ni	Mo
Austenite	68.31	17.46	11.32	2.91
δ-ferrite	70.29	25.03	4.68	–

Table 3. Results of EDX analysis (Figs. 4 and 5) of the weld metal/heat affected zone, wt.%

	Fe	Cr	Ni	Mn	Mo	Ti	O	Ca	Al	Si	Mg	S
Austenite	68.44	15.72	10.84	2.14	2.85	–	–	–	–	–	–	–
δ-ferrite	67.80	21.09	8.37	–	2.67	–	–	–	–	–	–	–
Inclusion 1	30.09	9.04	4.16	7.75	–	–	23.75	9.34	6.27	5.49	3.29	0.82
Inclusion 2	70.05	17.67	11.54	–	–	–	–	–	–	0.29	–	1.35
Inclusion 3	13.39	6.46	2.26	17.33	–	1.85	29.84	9.25	4.02	12.08	2.91	0.60

Table 4. The mass values for the AISI 316L steel samples before and after immersion to 6 wt.% $FeCl_3 \times 6\ H_2O$

Sample	m_1 (g)	m_2 (g)	Δm (g)
BM	27.0255	26.7749	0.2506
WM/HAZ	26.9440	26.2324	0.7116

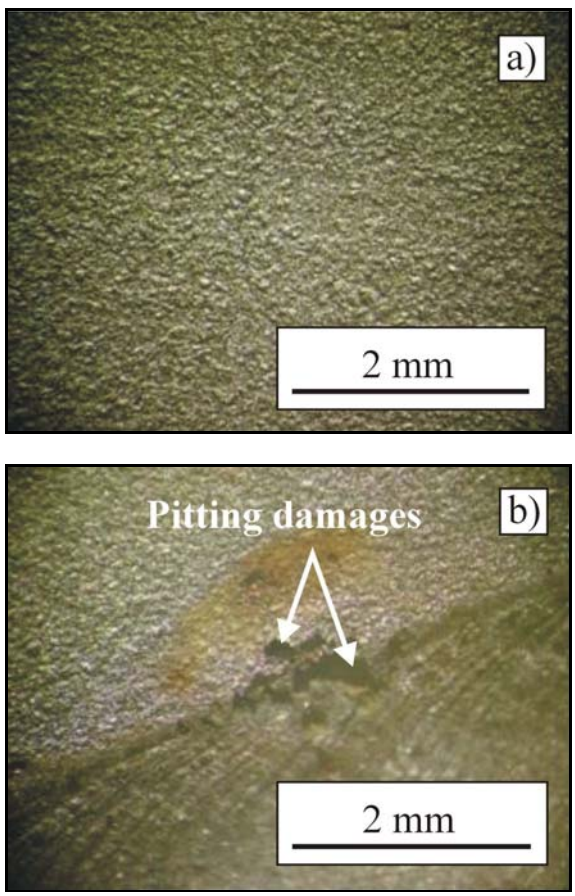

Fig. 6. Photographs of AISI 316L stainless steel surface for base metal (a) and at interface of the WM/HAZ (b) after the gravimetric measurements.

for the base metal. The current density of the base metal was similar to the sample taken from the interface of the WM/HAZ. The difference between E_{pit} and E_{pp} was used for determination of the passive

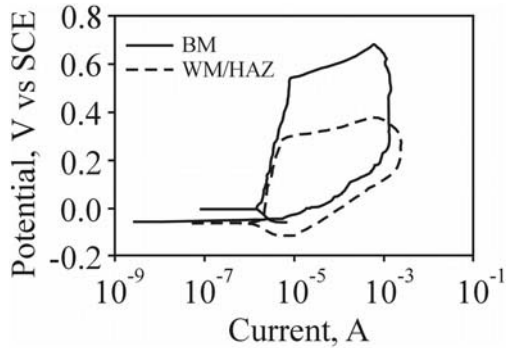

Fig. 7. Cyclic polarization curves of AISI 316L in 0.5 mol dm^{-3} NaCl solution. BM – base metal, WM/HAZ – *weld metal/heat affected zone.*

area width. The base metal showed the widest passive area (0.548 V) which confirmed that this material had the highest resistance of pitting corrosion. These results were in a good agreement with our results of gravimetric examinations. Lee et al. [18] suggested that such results of cyclic polarization could be supported by the following three findings: (a) the crack opening exerted a detrimental effect on the pitting corrosion resistance and pitting was initiated at the weakest regions, (b) while delta ferrite increased during the welding process, many chromium depleted zones were probably formed due to microsegregation of chromium at the ferrite-austenite interphase boundaries, leading to an increase of pitting susceptibility, and (c) the WM/HAZ was determined to be in cathodic position by the galvanic effect because the base metal showed more active potential. Also, Liqing et al. [19] studied the corrosion resistance of 316L steel as unwelded and as welded joint and concluded that the decrease of both the self-corrosion potential and the pitting potential of the welded 316L appeared which implied depression of the corrosion resistance of the welded joint.

After the cyclic polarization measurements, the surface of the electrodes was examined by optical and scanning electron microscopies. Optical and SEM micrographs of the surface of AISI 316L steel samples are shown in Figs. 8 and 9.

The pitting corrosion appeared on the surface of both samples of AISI 316L stainless steel electrodes.

Table 5. Critical potentials and protection intervals values obtained for AISI 316L steel samples in 0.5 mol dm^{-3} NaCl solution

Sample	E_{corr} (V)	E_{pp} (V)	E_{pit} (V)	E_{rp} (V)	$E_{pit} - E_{pp}$ (V)	$E_{pit} - E_{corr}$ (V)
BM	–0.005	0.004	0.543	–0.045	0.539	0.548
WM/HAZ	–0.061	–0.046	0.291	–	0.337	0.352

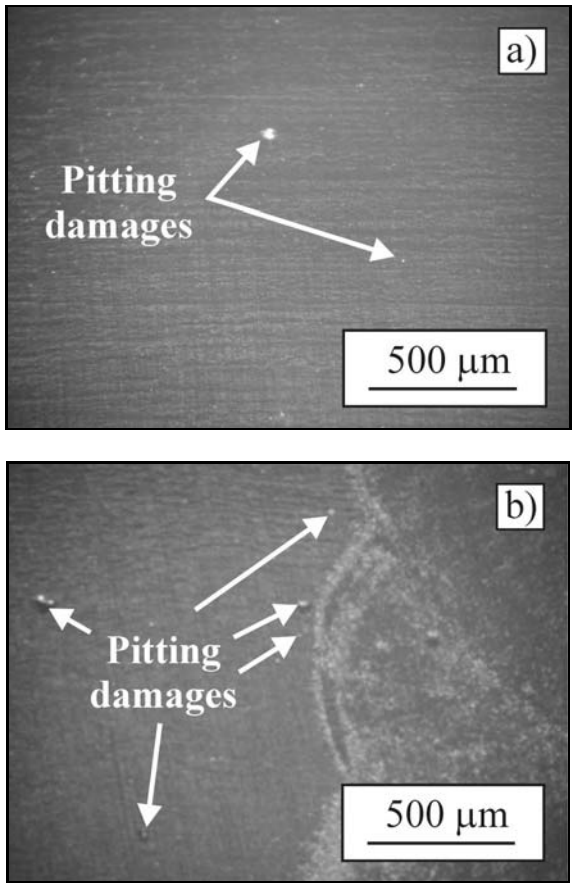

Fig. 8. Optical micrographs of the AISI 316L steel surface after cyclic potentiodynamic polarization in 0.5 mol dm^{-3} NaCl solution at 20 °C: a) sample of base metal, b) sample at interface of the WM/HAZ.

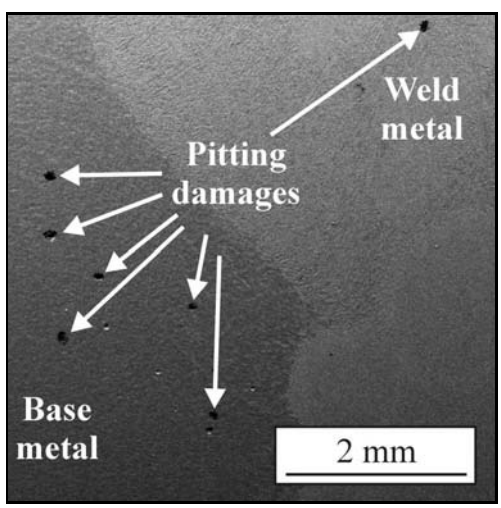

Fig. 9. SEM micrograph at the interface of the WM/HAZ of AISI 316L steel surface after cyclic potentiodynamic polarization in 0.5 mol dm^{-3} NaCl solution at 20 °C.

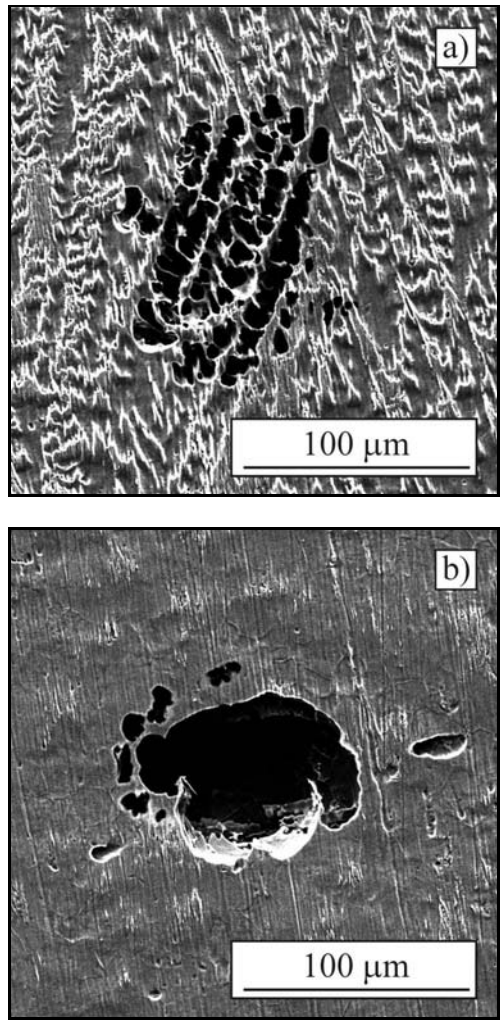

Fig. 10. SEM micrographs of the weld metal (a) and the heat affected zone (b) of AISI 316L steel surface after cyclic potentiodynamic polarization in 0.5 mol dm^{-3} NaCl solution at 20 °C.

The lowest number of pits could be found on the surface of the base metal while the surface of the sample which included interface of the WM/HAZ was significantly damaged by pitting corrosion. The pitting morphology in the weld metal and in the heat affected zone revealed localized and intense corrosion attack, Fig. 10. Figure 10 shows that grouped small pits occur on the surface of the weld metal, while in the heat affected zone these pits are greater and deeper.

Grain boundary movement caused by thermal cycling during welding in region of the WM/HAZ provides for more grain boundaries acting as sites for impurity atoms and these results in more segregation sites. The deterioration of corrosion properties often commonly associated with welding processes of austenitic stainless steels is related with the occurrence of segregations in microstructure. Also, Cui and Lundin

[20] mention that overlapped regions are usually the weakest sites to resist corrosion attack in the weld metal. In the case of the multi-run weld, each subsequent weld thermal cycle effectively affects a part of previous weld metal. This results in two regions with different microstructures: high temperature and low temperature regions. The differences in properties and microstructure of these regions often can result in preferential galvanic attack.

The corrosion of the weld metal and the heat affected zone was due to galvanic effect between inter-dendrite chromium-rich delta ferrite (21.09 % Cr, 8.37 % Ni) and the nickel-rich austenite (15.72 % Cr, 10.84 % Ni) in the area of the WM/HAZ (Fig. 4, Table 3). Also, SEM and EDX analysis before corrosion testing showed that in microstructure of the weld metal and the heat affected zone inclusions were present sporadically. These inclusions mainly consisted of oxygen, calcium, aluminum, silicon, magnesium and sulfur (Table 4), and they can be the main reason for pitting initiation at interface of the WM/HAZ. This coincides with the results of Zahrani et al. [17] which indicated that pitting initiation in the heat affected zone and in the weld metal of 316L steel might be attributed to the existence of large inclusions (rich with aluminum, silicon and sulfur) in the welded area and presence of the galvanic effect between delta ferrite and austenite.

Garcia et al. [21] mentioned that the pitting mechanisms of austenitic stainless steels were always related to the breakdown of the passive film. The protective role of the passive film depends on its composition and structure. Therefore we can expect that the changes in microstructure and composition due to welding affect the pitting corrosion behavior. Related to this fact, it is expected that inclusions with lower content of chromium (6.46 and 9.04 wt.%) observed in this work would be the main factor for the appearance of pitting.

In contrast, Dadfar et al. [22] suggested that the cooling process in TIG welding is so fast that the diffusion of alloying elements during welding is suppressed. Since the elements in the weld metal are uniformly distributed, both ferrite and austenite possess the same composition, so that delta ferrite in microstructure is not detrimental to the corrosion resistance. Transformation of the primary delta ferrite to austenite with ferrite-austenite solidification mode is diffusion controlled process. Fast cooling of welded joint during TIG process does not offer sufficient time to complete the phase transformation of ferrite to austenite. As a result, a large portion of primary delta ferrite is retained in the weld metal. Also, the higher heat input during welding would result in coarser delta ferrite grains. It affects that the passive film on the surface possesses low stability.

4. Conclusions

Results of the investigation into the corrosion failure and microstructure of high-alloyed AISI 316L austenitic stainless steel before and after welding allow to draw the following conclusions:

– The base metal consisted mainly of polygonal austenite grains and a small amount of delta ferrite. The delta ferrite content in the base metal was 0.4 % as compared to 10.6 % in the weld metal. The area of the weld metal contained a continuous network of vermicular and lathy type of ferrite with ferrite-austenite solidification mode.

– The smallest weight loss (0.2506 g) was observed on the sample of the base metal, while the highest mass loss (0.7116 g) suffered at the interface of the WM/HAZ.

– The base metal showed the widest passive area ($E_{pit} - E_{corr} = 0.548$ V) which confirmed that this material had the highest resistance of pitting corrosion in relation to the WM/HAZ ($E_{pit} - E_{corr} = 0.352$ V).

– SEM and EDX analysis before corrosion testing showed that inclusions were sporadically present in the microstructure of the weld metal and the heat affected zone. These inclusions mainly consisted of oxygen, calcium, aluminum, silicon, magnesium and sulfur and they can be the main reason for pitting initiation in the WM/HAZ.

– Also, the corrosion of the weld metal and the heat affected zone may be due to the galvanic effect between inter-dendrite chromium-rich delta ferrite (21.09 % Cr, 8.37 % Ni) and the nickel-rich austenite (15.72 % Cr, 10.84 % Ni) in the area of the WM/HAZ.

References

[1] Juraga, I., Šimunović, V., Stipaniček, Đ.: Metalurgija, *46*, 2007, p. 185.
[2] Gojić, M., Marijan, D., Tudja, M., Kožuh, S.: Materials and Geoenvironment, *55*, 2008, p. 408.
[3] Kulušić, B., Krstulović, Lj., Ivić, J.: Kemija u industriji, *53*, 2004, p. 1.
[4] Das, C. R., Bhaduri, A. K.: Engineering Failure Analysis, *10*, 2003, p. 667. doi:10.1016/S1350-6307(03)00062-1
[5] Lula, R. A.: Stainless Steel. Metals Park, Ohio, American Society for Metals 1986.
[6] Guan, K. S., Xu, X. D., Zhang, Y. Y., Wang, Z. W.: Engineering Failure Analysis, *12*, 2005, p. 623. doi:10.1016/j.engfailanal.2004.05.008
[7] Gojić, M., Marijan, D., Kožuh, S., Sorić, T.: Kemija u industriji, *58*, 2009, p. 253.
[8] Kožuh, S., Gojić, M., Kraljić Roković, M.: Chemical and Biochemical Engineering Quarterly, *22*, 2008, p. 421.
[9] Gojić, M., Marijan, D., Kosec, L.: Corrosion, *56*, 2000, p. 839. doi:10.5006/1.3280587

[10] Nishimoto, K., Ogawa, K.: Welding International, *13*, 1999, p. 845. doi:10.1080/09507119909452061
[11] Gooch, T. G.: Welding Journal, *5*, 1996, p. 135.
[12] Tavares, S. S. M., Corte, J. S., Menezes, C. A. B., Menezes, L., Moura, V., Corte, R. R. A.: Engineering Failure Analysis, *16*, 2009, p. 552. doi:10.1016/j.engfailanal.2008.05.008
[13] Fang, Z., Wu, Y., Zhu, R.: Corrosion, *50*, 1994, p. 171. doi:10.5006/1.3293508
[14] Krishnan, K. N., Prasad, R. K.: Materials Science and Engineering, *A142*, 1991, p. 79. doi:10.1016/0921-5093(91)90756-D
[15] ASTM G48-03, Standard Test Methods for Pitting and Crevice Corrosion Resistance of Stainless Steels and Related Alloys by Use of Ferric Chloride Solution. ASTM International, USA 2003.
[16] Gojić, M.: Techniques of Joining and Cutting of Materials. Sisak, University of Zagreb Faculty of Metallurgy 2003 (in Croatian).
[17] Zahrani, E. M., Saatchi, A., Alfantazi, A.: Engineering Failure Analysis, *17*, 2010, p. 810. doi:10.1016/j.engfailanal.2009.10.015
[18] Lee, D. J., Jung, K. H., Kim, Y. H., Lee, K. H., Park, J. U., Shin, Y. T, Lee, H. W.: Materials and Design, *30*, 2009, p. 3269. doi:10.1016/j.matdes.2009.01.023
[19] Liqing, H., Guobiao, L., Zidong, W., Hong, Z., Feng, L., Long, Y.: Rare Metal Materials and Engineering, *39*, 2010, p. 393.
[20] Cui, Y., Lundin, C. D.: Materials Letters, *59*, 2005, p. 1542. doi:10.1016/j.matlet.2005.01.018
[21] Garcia, C., Martin, F., De Tiedra, P., Blanco, Y., Lopez, M.: Corrosion Science, *50*, 2008, p. 1184. doi:10.1016/j.corsci.2007.11.028
[22] Dadfar, M., Fathi, M. H., Karimzadeh, F., Dadfar, M. R., Saatchi, A.: Materials Letters, *61*, 2007, p. 2343. doi:10.1016/j.matlet.2006.09.008